Volume Imaging of an Ultrathin SBS Triblock Copolymer Film

Matthias Konrad, Armin Knoll, Georg Krausch, and Robert Magerle*

Lehrstuhl für Physikalische Chemie II, Universität Bayreuth, 95440 Bayreuth, Germany

Received December 8, 1999

ABSTRACT: We use scanning force microscopy and stepwise erosion in a radio-frequency (rf) plasma to obtain a three-dimensional volume image of an ultrathin poly(styrene-*b*-butadiene-*b*-styrene) triblock copolymer film. The free surface of the film exhibits domains of two distinctly different structures, i.e., hexagonal arrays of isolated dots and parallel stripes. A common forehand interpretation relates these surface morphologies to a cylindrical microdomain morphology with the cylinders oriented perpendicularly and parallel to the plane of the film, respectively. In contrast, our experiments show that the "dots" merge into parallel cylinders at some distance underneath the film surface. These results demonstrate that care has to be taken when the thin film morphology of block copolymers is inferred from their surface structure.

Introduction

Block copolymers represent an interesting class of materials due to their potential to self-assemble into highly ordered microdomain morphologies with characteristic dimensions on the molecular scale.[1,2] While the bulk of such materials is often characterized by a multidomain structure resembling the situation in polycrystalline materials, the microdomain morphology of thin copolymer films has been found to be strongly influenced by the boundary surfaces.[3−5] It was shown that small differences in interfacial energy between the different blocks at both the substrate surface and the free surface tend to align the resulting microdomains. In the case of symmetric diblock copolymers, effective alignment of the lamellae parallel to the plane of the films was observed.[3] In addition, geometrical constraints have been found to play a decisive role in thin films whenever the film thickness is of the same order of magnitude as the characteristic equilibrium domain size.[6−8]

While thin films of symmetric diblock copolymers have been studied quite extensively over the past 10 years,[5] the more complex situation of asymmetric AB diblock and ABA triblock copolymer thin films has only rarely been investigated.[8−14] First studies of surfaces and thin films of block copolymers containing more than two species have only recently been reported.[15,16] In contrast to the effectively one-dimensional nature of a perfectly aligned lamellar structure, the more complex systems tend to form more complex three-dimensional microdomain morphologies even in thin film geometry. Moreover, the symmetry of the bulk domain morphologies will generally be broken at the interfaces confining the film, e.g., by a wetting layer of one of the polymer components.[8,9,11] The situation becomes even more involved when defects and nonequilibrium morphologies have to be taken into account. In all these cases, experimental tools are needed which provide a three-dimensional volume image of the thin film morphology with a spatial resolution in the nanometer regime.

Plane-view transmission electron microscopy (TEM) can be used for thin film studies provided that the films can be prepared on TEM grids[8] or transferred from the substrate of interest onto the grid.[11,12] However, only projections along a given axis (typically the surface normal) are obtained, and composition variations along this axis are difficult to analyze. Such variations can be imaged by cross-sectional TEM, however, on cost of the lateral information within the plane of the film. Various depth profiling techniques are available to study the (laterally averaged) material distribution perpendicular to the plane of the film[17] with high spatial resolution. In principle, a suitable combination of such techniques does allow to establish the full three-dimensional morphology of a perfectly ordered block copolymer film. The same holds when techniques such as scanning electron microscopy (SEM) and scanning force microscopy (SFM) are combined with layer by layer removal of the films, e.g., by plasma etching.[18−20] One has to realize, though, that details of defects and partly disordered structures are only accessible when the same area of the specimen is imaged after successive erosion steps.

In the present paper, we apply the recently developed nanotomography technique[21] to image the details of the three-dimensional morphology of a thin film of poly(styrene-*b*-butadiene-*b*-styrene) (SBS). Nanotomography is based on a combination of SFM imaging and stepwise erosion of the sample in a rf plasma. Both the surface topography and some sort of material contrast are determined at a given area of the sample after each erosion step. Therefore, neither large-scale surface topography features inherent in the sample nor surface roughness limits the imaging capabilities, and in contrast to earlier work,[18−20] a three-dimensional volume image of the material distribution within a certain volume of the specimen can be reconstructed.

The bulk equilibrium morphology of the material under study is a hexagonal array of polystyrene (PS) cylinders embedded within a polybutadiene (PB) matrix.[22] In thin films, two possible morphologies have been reported in the literature, with the cylinder axes lying in plane or standing perpendicular to the plane of the film[11−14] (Figure 1). Because of the large difference in the glass transition temperature between PS and PB, the material distribution in the near-surface region of the films can easily be determined by phase contrast

* Corresponding author. E-mail: robert.magerle@uni-bayreuth.de.

10.1021/ma992057f CCC: $19.00
Published on Web 06/28/2000

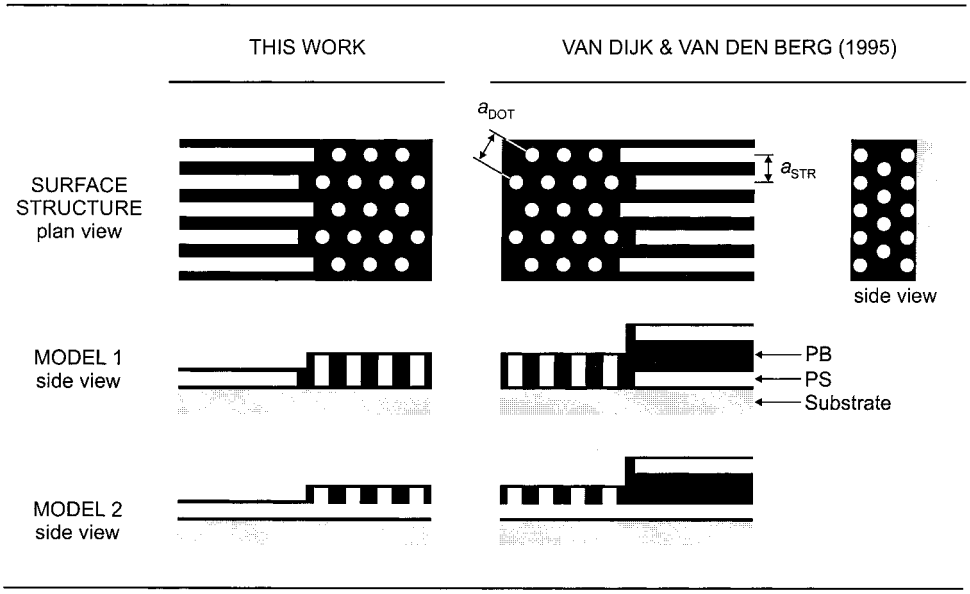

Figure 1. Schematic presentation of possible thin film morphologies of block copolymers exhibiting a cylindrical mircodomain structure. The left-hand side shows the thickness regime studied in the present work, while the right-hand side refers to the thickness regime studied by van Dijk and van den Berg.[13] The top part shows the surface morphologies corresponding to different film thicknesses as they typically appear in SFM TappingMode phase images. The two models show different "bulk" morphologies of the films which lead to the same surface structure. Model 1 was suggested by van Dijk and van den Berg,[13] while model 2 is based on the experimental results described in the present work.

TappingMode SFM measurements.[14] As indicated schematically in Figure 1, regularly spaced, stripelike patterns are typically obtained, if the cylinders lie parallel to the film surface. In contrast, if the cylinders are oriented perpendicular to the film surface, the SFM phase images are characterized by a hexagonal array of dots (i.e., the cylindrical cores) embedded in a continuous second phase (i.e., the matrix phase). It is commonly accepted that the reverse conclusion is valid as well, and accordingly, surface morphologies obtained by SFM have been used to establish volume morphologies.[13] As we shall show in the following, this conclusion need not be correct; i.e., the observation of a hexagonal array of dots at the film surface *does not* necessarily imply that the film morphology consists of cylinders standing perpendicular to the plane of the film. We shall discuss this finding in view of the published literature on this system.

Experimental Section

Poly(styrene-*b*-butadiene-*b*-styrene) (SBS) was obtained from Polymer Source Inc. The PS, PB, and PS blocks had weight-averaged molecular weights of 14K, 73K, and 15K, respectively, and a polydispersity of 1.02. In bulk the PS blocks self-organize into cylinders of about 24 nm diameter embedded within a PB matrix. Viewed along their long axes, the cylinders form a hexagonal lattice with a mean distance of ≈42 nm between two next-nearest cylinders. An SBS film was prepared on a polished silicon wafer by spin-casting (2500 rpm) from a 1 wt % toluene solution. For equilibration and long-range ordering of the SBS microdomain structure the sample was exposed to saturated chloroform vapor for 30 min.

The lateral distribution of PS and PB near the film surface was imaged with scanning force microscopy (SFM) operated in TappingMode. All experiments were performed on a Digital Instruments Dimension 3100 scanning force microscope using standard Silicon cantilevers (NANO*SENSORS* Dr. Olaf Wolter GmbH). The free amplitude of the cantilever was set to about 35 nm, and a set-point ratio of about 95% was chosen. A phase image $\varphi(x,y)$ was recorded in addition to the surface topography $z(x,y)$. Some of the SFM data (Figure 3) were flattened (third order) and filtered (low pass) to improve the image quality. The phase images reflect lateral differences in the mechanics of the tip−sample interaction which differs considerably between PS and PB due to the large difference in their glass transition temperatures T_g.[14] At room temperature PS ($T_g \approx 100$ °C) is much stiffer than PB (with 1,4-addition $T_g \approx -105$ °C). Therefore, the phase image can be interpreted as a high-resolution map of the near-surface distribution of PS and PB.

For volume imaging thin layers of the block copolymer were successively removed by plasma etching, and TappingMode SFM images were taken at the same spot after each etching step.[21] A spot was chosen with characteristic landmarks within and nearby the imaged area which helped finding the same spot again after ex-situ plasma etching. For plasma etching the specimen was placed in a Harrick PDC-32G plasma cleaner which was then operated with air at 1.5 mbar pressure and 60 W rf power for 25 s. The average etch rate amounted to 6.7 nm per step. The result of this procedure is a stack of TappingMode phase images $\varphi_n(x,y)$ reflecting the material distribution near the surfaces $z_n(x,y)$ (n is an integer). From this stack of images, a three-dimensional volume image of the PS and PB distribution was reconstructed.

Results

In Figure 2a, we show an SFM topography image exhibiting the coarse grain morphology of the SBS film after exposure to chloroform vapor. The film develops two distinct thicknesses of some 70 nm (bright areas) and 45 nm (dark areas). Each film thickness is characterized by a distinct surface micromorphology. This can be seen in Figure 2b, where the phase contrast image of a 2.5 × 2.5 μm^2 detail of Figure 2a is shown. The surface of the thicker regions is characterized by an array of isolated dark dots in a continuous gray background. The surface of the thinner regions, on the other hand, is characterized by a stripelike pattern of gray and dark stripes. The average distance between the stripes amounts to 39.8 ± 0.8 nm (see Table 1). We may

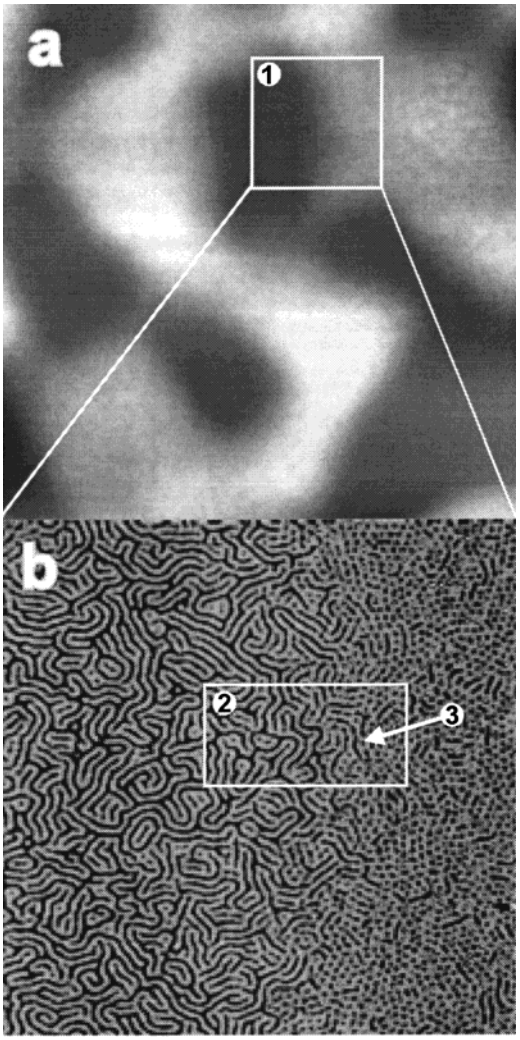

Figure 2. (a) SFM TappingMode topography image (10 × 10 μm^2) of a thin SBS triblock copolymer film after treatment in chloroform vapor. The gray scale ranges from 0 to 50 nm. (b) SFM TappingMode phase contrast image of the detail of (a) indicated by the white box (2.5 × 2.5 μm^2). The gray scale ranges between 0 and 10°.

identify the dark regions in the phase image as PS microdomains. This assignment is based on the fact that PS is the minority component in the block copolymer and that it is therefore expected to form isolated microdomains in a continuous PB matrix phase. The assignment is further corroborated by comparison with phase images of PS/PB homopolymer blends investigated under identical imaging conditions at light tapping (set point ≈ 99−95%), where the PS domains appear darker than the PB domains. At harder tapping conditions, i.e., at smaller set points, PS appears brighter than PB.

So far our experimental findings resemble the results of van Dijk and van den Berg,[13] who studied thin films of a similar material. They also reported the spontaneous formation of different film thicknesses characterized by stripes and dots, respectively. The authors explained their results by the assumption that the dotted surface morphology relates to cylinders oriented perpendicular to the plane of the film. This orientation should occur whenever the film thickness does not allow to accommodate an integer number of layers of lying cylinders (see Figure 1, model 1). Following the same reasoning, the data shown in Figure 2b could also be explained by

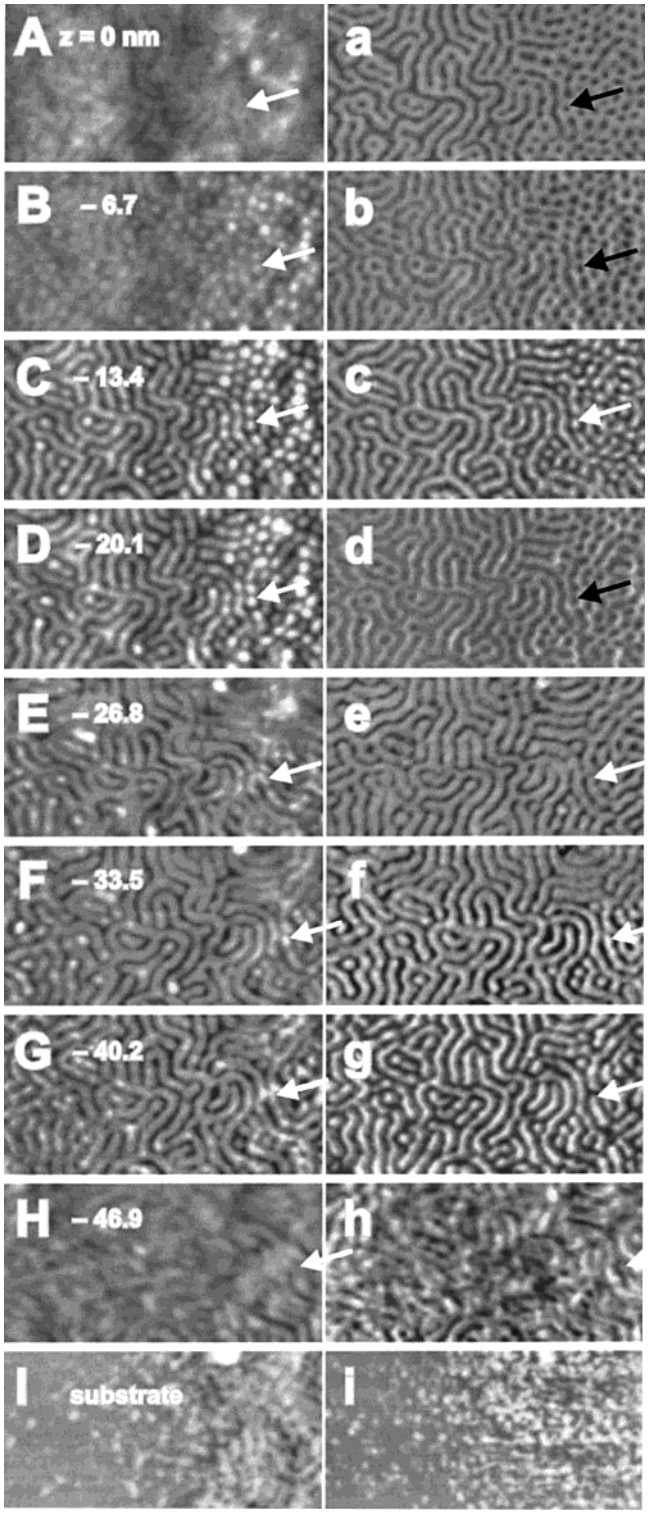

Figure 3. SFM TappingMode topography (A−H) and phase (a−h) images prior to plasma etching (A, a) and after succesive etching steps (B−H, b−h). The average etching depth is indicated in the top left of the topography images. The imaged area is 0.5 × 1 μm^2. The location of this area is indicated by the white box in Figure 2b.

two different cylinder orientations, i.e., parallel to the plane of the film (in the thinner regions) and perpendicular to the plane of the film (in the thicker regions).

To check the above hypothesis experimentally, we have investigated a smaller area of the film (indicated by the white box in Figure 2b) by nanotomography.[21] The investigated area was chosen such that it contained

Table 1. Film Thickness *h*, Distance between Next-Nearest Stripes (a_{STR}) and Dots (a_{DOT}), and Ratio a_{DOT}/a_{STR}

	h (nm)	a_{STR} (nm)	a_{DOT} (nm)	a_{DOT}/a_{STR}
		This Work		
Figure 2	45 ± 2	39.8 ± 0.8		1.09 ± 0.03
	45−60		43.5 ± 0.9	
		van Dijk and van den Berg (1995)[a]		
Figure 1[a]	140 ± 2[a]	31.1 ± 0.6[a]	36.5 ± 2.5[b]	1.17 ± 0.08
Figure 3[a]	42 ± 1[a]		35.9 ± 0.6[c]	1.15 ± 0.03[d]
Figure 5[a]	39[a]		38.4 ± 0.8	1.22 ± 0.03
	64[a]	31.5 ± 0.4		

[a] Reference 13. [b] Only very few dots are present in Fig. 1 of ref 13. Therefore, the error of this value is larger than that of the other values. [c] Value given in ref 13 multiplied by 1.155. [d] Determined assuming $a_{STR} = 31.1 \pm 0.6$ nm.

regions of both stripes and dots. For volume imaging, the sample was removed from the SFM, exposed to the rf plasma for 25 s, and imaged again. This procedure was repeated eight times. After the sixth plasma etching step, the remaining film thickness was determined relative to the underlying substrate. From this value an average etching rate of 16 ± 0.7 nm/min and an etching depth of 6.7 ± 0.3 nm/step were calculated. The average etching rate agrees well with the etching rates of the respective homopolymers, weighted by the volume ratio between the two blocks. The etching rates of PS and PB homopolymers were determined in separate experiments to 9.8 ± 0.4 and 19.7 ± 0.5 nm/min, respectively. The result of the nanotomography experiment is displayed in Figure 3, where topography and phase images are shown prior to etching (Figure 3A,a) and after successive etching steps (Figure 3B−H,b−h).

Before we discuss the data in detail, we point to the major qualitative result of this experiment. Prior to etching and after the first few etching steps (Figure 3A,a−D,d), the right half of the phase images is characterized by a "dotted" morphology. After successive etching, however, the stripelike pattern extends over the entire area of the images, and hardly any isolated dotlike structures are visible. This finding clearly contradicts the above assumption that the dots relate to cylinders oriented perpendicular to the plane of the film (Figure 1, model 1). The microdomain morphology of the film is obviously more complex involving "lying" cylinders close to the substrate and some characteristic near-surface morphology leading to the observed dotted surface structure. A schematic structural model based on this finding is depicted in Figure 1, model 2. Model 2 is further corrobated by the fact that pure PB is etched faster than pure PS. Therefore, after etching of SBS the PS domains form protrusions, and in particular the PS necks on PS cylinders become clearly visible in the topography images shown in Figure 3B−D. In particular, our results demonstrate that measurements of the surface structure alone do not allow to draw straightforward conclusions on the "bulk" morphology of a thin film.

Despite this unambiguous result, the data displayed in Figure 3 (the phase images in particular) bear some peculiarities caused by the TappingMode technique. At first, we find that details of the microdomain morphology are well resolved in the SFM images, and one can follow these details from image to image through successive etching steps. Characteristic defects, e.g., in the stripe pattern visible in the left half of the images, are seen throughout the entire set of images, clearly demonstrating that the same spot has been imaged throughout the procedure. While this finding demonstrates the general feasibility of the experimental approach, the same set of data unravels some characteristic problems which occur if one tries to image the same spot of a sample several times using SFM TappingMode phase imaging. While Figure 3a,b,d is characterized by isolated dark dots, in Figure 3c,e,f,g the same area exhibits isolated bright dots in the phase image. This problem of "phase inversion" is a common phenomenon in SFM studies of polymer surfaces;[14,23,24] however, it is rarely discussed in detail. In general, the phase signal on soft surfaces is determined by both parameters characterizing the oscillating tip (such as sharpness, quality factor of the cantilever, its absolute amplitude, and drive frequency) and parameters describing the surface (stiffness, viscoelasticity, adhesion). In additon, parameters characterizing the feedback loop and the scanning speed of the tip also play a role. If all parameters are kept constant, the sign and magnitude of the phase signal can be controlled by the cantilever amplitude set point in a reproducible way.

The nanotomography approach chosen here requires that the same spot of the samples is imaged many times with very high quality, despite the fact that the sample is removed from the SFM and treated in a plasma between successive imaging steps. In this situation it appears extremly difficult to keep all parameters constant. We observe that tiny changes of the set point between successive etching steps can easily lead to the observed phase inversion. Uncontrolled changes in the surface chemical composition due to the plasma etching add to the problem of establishing identical imaging conditions after each etching step. In addition, the conditions of the tip (e.g., temporary take-up of some polymeric material) may change as well in an uncontrolled manner.[25]

The phenomenon of phase inversion (which is more likely to occur under light tapping conditons) as well as the fact that the contrast in the phase images varies from image to image has to be taken care of before a three-dimensional image can be reconstructed from the data displayed in Figure 3. Since we are interested in the spatial distribution of the PS/PB ratio f (which varies between 0 and 1), we take a pragmatic approach and assume the measured phase image $\varphi_n(x,y)$ to be a linear function of the PS/PB ratio $f_n(x,y)$, i.e., $\varphi_n(x,y) \approx \varphi_A f_n(x,y) + \varphi_0$. The two parameters φ_A and φ_0 depend on the actual tapping conditions and may change from image to image (see Figures 2 and 3 and the discussion above). Since the average etching step (6.7 nm) is considerably smaller than a typical block copolymer domain size (24 nm), the maps of the PS/PB ratio are expected to change continuously from image to image. Therefore, for further processing, the contrast of the phase images in Figure 3a,b,d was inverted. By this means, in all images bright and dark areas correspond to PS and PB microphases, respectively. Furthermore, we subtract the average phase value φ_0 from each scan line by fitting a third-order polynomial to it and subtracting it thereafter. This "flatten" procedure corrects for changes in φ_0 and results in an average value $\langle\varphi_n(x,y)\rangle = 0$ in all images.[26] Finally, all phase images were normalized to a constant standard deviation of the phase about $\langle\varphi_n(x,y)\rangle = 0$ in order to establish the same phase contrast in all images. This corrects for differences in φ_A between different images and results in a

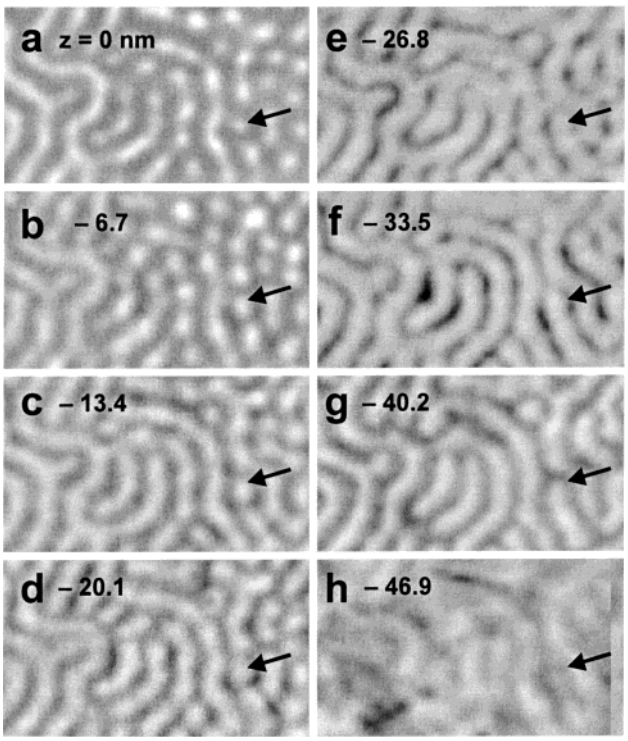

Figure 4. SFM TappingMode phase images of a detail around the arrows in Figure 3 after normalization of the phase values and image registration (see text). The black arrow indicates the reference points used for image registration. The black numbers indicate the average etching depth relative to the original surface of the film.

quite uniform mapping of gray values to the PS/PB-ratio $f_n(x,y)$. For image registration (alignment), reference points (arrows in Figure 3) have been chosen such that the correlation coefficient between areas around the reference points in successive images is maximized.[27] The images were aligned by lateral displacements according to these reference points. In Figure 4 we show the resulting set of phase images after normalization and registration. The black arrows indicate the respective reference points.

For three-dimensional representation, the phase distribution $\varphi(x,y,z)$ was determined by combination of the information contained in the *normalized* phase images $\varphi_n(x,y)$ with the information on the respective topography images $z_n(x,y)$. From $\varphi(x,y,z)$ we calculated the isosurfaces surrounding the points (x,y,z) with a phase value $\varphi(x,y,z) > \varphi_t$. φ_t is a threshold value, which was set to zero in the present case. The enclosed volume can then be interpreted as the PS microdomains. The resulting three-dimensional image of the sample is displayed in Figure 5. Wherever the boundary surfaces of the imaged volume cut through a region with $\varphi > \varphi_t$, the color relates to the normalized value of the phase at the respective surface. As an example, the gray values at the top surface of the volume displayed in Figure 5 relate to the phase image of the untreated surface of the film (Figure 4a). Figure 5 nicely demonstrates the feasibility of the nanotomography approach for three-dimensional imaging of polymeric microstructures with a spatial resolution of some nanometers along all three spatial directions. Although Figure 5 does not add any new information beyond Figures 3 and 4, we want to emphasize that the use of image processing software is of great advantage for the analysis of the data $\varphi(x,y,z)$ obtained from the SFM images. By choosing different

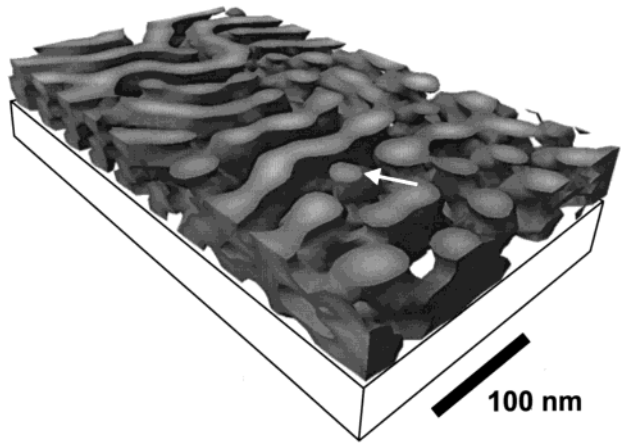

Figure 5. Three-dimensional representation of the phase values $\varphi(x,y,z)$ reconstructed from the data displayed in Figure 4 and the corresponding topography images. The isosurface surrounds the regions with $\varphi(x,y,z) > 0$.

viewpoints, color tables, and phase threshold values φ_t, the detailed three-dimensional microdomain structure can be investigated in a much easier comprehendible way then just by looking at the series of SFM images as displayed in Figures 3 and 4. These advantages become very obvious by interactive visualization of the data on a suitable computer.

Discussion

We now return to a discussion of the central result of the data displayed in Figures 3−5. We observe a complete layer of cylinders oriented parallel to the substrate which in thicker regions of the film develop necks extending to the film surface. The resulting thin film structure is schematically depicted in Figure 1 (model 2). Our experimental finding clearly contradicts the notion of entire cylinders oriented perpendicular to the plane of the film as put forward in ref 13 (Figure 1, model 1). Furthermore, if the dots observed at the sample surface correspond to necks evolving from lying cylinders underneath, they have to be organized in rows with a characteristic inter-row distance equal to the distance between the stripes a_{STR}. This is indeed observed in our experiments as well as in the experiments by van Dijk and van der Berg.[13] Consequently, since the dots exhibit some hexagonal order, the nearest-neighbor distance between dots, a_{DOT}, must differ from the nearest-neighbor distance between stripes by a geometrical factor of $(a_{DOT}/a_{STR}) = 2/\sqrt{3} \approx 1.155$. This is in agreement with a quantitative analysis (see Table 1) of the SFM data shown in Figure 2 as well as the data of van Dijk and van den Berg (Figures 1, 3, and 5 in ref 13). Although van Dijk and van den Berg stated that the spacing between dots and stripes was equal, careful analysis of their SFM images shows that this is not the case. Evidently, the authors misinterpreted the 2D Fourier transforms of the hexagonal dot structure. Indeed, the Fourier transforms revealed a characteristic spacing equal to the spacing observed between stripes on the surface. It has to be realized, however, that the characteristic peaks in the 2D Fourier transform of a hexagonal lattice correspond to the distance between lines of dots (which is equal to $a_{DOT}\sqrt{3}/2$) rather than to the dot−dot nearest-neighbor distance a_{DOT}. The ratio between the two amounts to the factor $\sqrt{3}/2$, so the error canceled and the authors were not led to question their results.

We summarize that both our own experiments and the earlier work on SBS thin films[13] show that the nearest-neighbor distance between the dots (a_{DOT}) observed at certain film thicknesses is larger by a factor of $2/\sqrt{3}$ compared to the distance between the stripes (a_{STR}) in other regions of the film. If one assumed the bulk hexagonal packing of cylinders to be present in the thin film in two different orientations, this finding would imply that for at least one of the cylinder orientations a deformation with respect to the bulk structure is present throughout the *whole* film. Qualitatively, such a deformation will lead to a higher state of free energy of the system. It is therefore questionable whether such a situation is likely to occur at all in ultrathin films. In contrast, when necks form (model 2), only the topmost layer with a thickness corresponding to about one-half of a full cylinder layer deviates from bulk morphology.

It is worth mentioning that the sample preparation procedure carried out by van Dijk and van den Berg[13] (thermal annealing) differs quite significantly from the solvent vapor treatment used in the present work. The fact that the resulting surface structures are quantitatively similar to the ones described here indicates that the formation of "necks" emerging from parallel cylinders may indeed be a general phenomenon in thin SBS films. Further experiments using the nanotomography approach on thermally annealed samples of different film thickness will be needed to clarify this issue. For the present, we only note that immediate conclusions from surface morphology to volume structure are not straightforward and may lead to wrong results even in the case of "simple systems".

Conclusion

Using a novel combination of SFM imaging and plasma etching,[21] we were able to establish a three-dimensional real-space image of a thin SBS triblock copolymer film. We observe cylindrical microdomains oriented parallel to the substrate for a film thickness of about one cylindrical diameter. In thicker regions, these cylinders develop necks extending to the film surface. This work clearly demonstrates that care has to be taken when deducing bulk morphologies from measurements on the surface of a specimen. The method of nanotomography extends SFM measurements to real-space volume imaging. Together with suitable image processing routines, it can help visualize and understand complex mesophase morphologies in block copolymers, polymer blends, and related systems. This seems particularly interesting for the study of defects and nonperiodic structures as well as thin films.

Acknowledgment. The authors appreciate financial support through the Deutsche Forschungsgemeinschaft (SFB 481, TP B7).

References and Notes

(1) Bates, F. S.; Fredrickson, G. H. *Annu. Rev. Phys. Chem.* **1990**, *41*, 525.
(2) Bates, F. S.; Frederickson, G. H. *Phys. Today* **1999**, *52*, 32.
(3) Anastasiadis, S. H.; Russell, T. P.; Satija, S. K.; Majkrzak, C. F. *Phys. Rev. Lett.* **1989**, *62*, 1852.
(4) Russell, T. P.; Coulon, G.; Deline, V. R.; Miller, D. C. *Macromolecules* **1989**, *22*, 4600.
(5) Krausch, G. *Mater. Sci. Eng. Rep.* **1995**, *14*, 1.
(6) Coulon, G.; Collin, B.; Ausserre, D.; Chatenay, D.; Russell, T. P. *J. Phys. (Paris)* **1990**, *51*, 2801.
(7) Lambooy, P.; Russell, T. P.; Kellogg, G. J.; Mayes, A. M.; Gallagher, P. D.; Satija, S. K. *Phys. Rev. Lett.* **1994**, *72*, 2899.
(8) Radzilowski, L. H.; Carvalho, B. L.; Thomas, E. L. *J. Polym. Sci., Part B: Polym. Phys.* **1996**, *34*, 3081.
(9) Liu, Y.; Zhao, W.; Zheng, X.; King, A.; Singh, A.; Rafailovich, M. H.; Sokolov, J.; Dai, K. H.; Kramer, E. J.; Schwartz, S. A.; Gebizlioglu, O.; Sinha, S. K. *Macromolecules* **1994**, *27*, 4000.
(10) Jeu, W. H. d.; Lambooy, P.; Hamley, I. W.; Vaknin, D.; Pedersen, J. S.; Kjaer, K.; Seyger, R.; Hutten, P. v.; Hadzioannou, G. *J. Phys. II* **1993**, *3*, 139.
(11) Kim, G.; Libera, M. *Macromolecules* **1998**, *31*, 2569.
(12) Kim, G.; Libera, M. *Macromolecules* **1998**, *31*, 2670.
(13) van Dijk, M. A.; van den Berg, R. *Macromolecules* **1995**, *28*, 6773.
(14) Magonov, S. N.; Cleveland, J.; Elings, V.; Denley, D.; Whangbo, M. H. *Surf. Sci.* **1997**, *389*, 201.
(15) Stocker, W.; Beckmann, J.; Stadler, R.; Rabe, J. P. *Macromolecules* **1996**, *29*, 7502.
(16) Elbs, H.; Fukunaga, K.; Sauer, G.; Stadler, R.; Magerle, R.; Krausch, G. *Macromolecules* **1999**, *32*, 1204.
(17) Kramer, E. J. *Physica* **1991**, *B173*, 189.
(18) Harrison, C.; Park, M.; Chaikin, P. M. *Polymer* **1997**, *39*, 2733.
(19) Harrison, C.; Park, M.; Chaikin, P. M.; Register, R. A.; Adamson, D. H.; Yao, N. *Macromolecules* **1998**, *31*, 2185.
(20) Fukunaga, K.; Elbs, H.; Magerle, R.; Krausch, G. *Macromolecules* **2000**, *33*, 947.
(21) Magerle, R. *Phys. Rev. Lett.*, in press.
(22) Keller, A.; Odell, J. A.; Folkes, M. J. In *Processing, Structure, and Properties of Block Copolymers*; Folkes, M. J., Ed.; Elsevier: London, 1985; p 29.
(23) Bar, G.; Thoman, Y.; Brandsch, R.; Cantow, H.-J.; Whangbo, M.-H. *Langmuir* **1997**, *13*, 3807.
(24) Brandsch, R.; Bar, G.; Whangbo, M.-H. *Langmuir* **1997**, *13*, 6349.
(25) After each etching step we have taken images under "light" (set point ≈ 95%) and under "moderate" tapping conditions (set point ≈ 85%). The observed dependence of the phase contrast on the set point value is consistent with respective experiments on SBS films prior to etching as well as on films of PS/PB homopolymer blends. Most important for this work, phase images taken under light and moderate tapping conditions give practically identical results after the normalization procedure described below is applied. However, images taken under light tapping conditions suffer less from problems due to take-up of polymeric material and lead to "better micrographs". Therefore, we have chosen the images taken under light tapping conditions for display in Figure 3 and for 3D reconstruction.
(26) Formally, this is motivated by assuming φ_A to be a constant within one image, φ_0 to change slowly compared to $f_n(x,y)$, and the mean value of $f_n(x,y)$ to be the same in each scan line.
(27) Gonzales, P. C.; Woods, R. E. *Digital Image Processing*; Addison-Wesley: Reading, MA, 1992.

MA992057F